

A low-power, high-sensitivity micromachined optical magnetometer

R. Mhaskar,^{1,2} S. Knappe,^{1,2} and J. Kitching¹

¹*Time and Frequency Division, National Institute of Standards and Technology, 325 Broadway, Boulder, Colorado 80305, USA*

²*University of Colorado, Boulder, Colorado 80309, USA*

(Received 1 October 2012; accepted 26 November 2012; published online 11 December 2012)

We demonstrate an optical magnetometer based on a microfabricated ⁸⁷Rb vapor cell in a micromachined silicon sensor head. The alkali atom density in the vapor cell is increased by heating the cell with light brought to the sensor through an optical fiber, and absorbed by colored filters attached to the cell windows. A second fiber-optically coupled beam optically pumps and interrogates the atoms. The magnetometer operates on 140 mW of heating power and achieves a sensitivity below 20 fT/√Hz throughout most of the frequency band from 15 Hz to 100 Hz. Such a sensor can measure magnetic fields from the human heart and brain. © 2012 American Institute of Physics. [<http://dx.doi.org/10.1063/1.4770361>]

Optical (or atomic) magnetometers¹ are based on optical detection of the precession of an ensemble of electronic or nuclear spins in a magnetic field. Over the last fifteen years, considerable progress has been made in understanding the underlying physics that limits the performance of instruments based on room-temperature vapor cells. The best optical magnetometers currently achieve sensitivities below 1 fT/√Hz in both a low-field vector mode of operation² and a high-field scalar mode.³ The development of optical magnetometers using new excitation methods,⁴ new mechanisms that reduce spin relaxation,^{5,6} and in new atomic systems such as Bose-Einstein condensates⁷ and nitrogen vacancy centers in diamond⁸ is also underway. In parallel, optical magnetometer sensor technology based on vapor cells has progressed considerably beyond what is currently available commercially. For example, fiber-optically coupled sensors have been developed⁹ for robust operation outside the laboratory and achieved a resolution under 1 pT. In addition “chip-scale” optical magnetometers¹⁰ based on microfabricated vapor cells have demonstrated a sensitivity of a few pT/√Hz in integrated physics packages of volume under 20 mm³.¹¹ Table-top measurements have shown that microfabricated vapor cells can support sensitivities of 5 fT/√Hz¹² in a low-field environment. Microfabricated sensor heads combine the fabrication and cost advantages of silicon micromachining with multi-sensor system scalability and non-magnetic and largely non-metallic design. Fiber-optic coupling to the sensor heads allows remotely located lasers and control/detection electronics to drive many sensors simultaneously while avoiding interference of electric-current-induced fields with the sensing volume. This sensor design has shown sensitivities in the pT/√Hz range in microtesla background fields¹³ and sub-pT/√Hz sensitivities in fields below 1 nT.¹⁴

One important emerging application of optical magnetometers is the measurement of magnetic fields produced by the human body, particularly those originating in the heart or brain. While high-sensitivity magnetometers based on Superconducting Quantum Interference Devices (SQUIDS) have traditionally dominated this field, optical magnetometers offer the considerable advantage that no cryogenic cooling is required. Both magnetocardiography (MCG)¹⁵ and magneto-

encephalography (MEG)¹⁶ with optical magnetometers have been demonstrated.

The signal to noise ratio of an optical magnetometer improves with increasing atomic density in the vapor cell. A higher cell temperature is therefore desirable. This is usually achieved by resistive heating of an electrical conductor surrounding or in contact with the vapor cell; these conducting elements produce residual, time-varying magnetic fields and noise. Optical heating through absorption of light by some element of the cell allows for sensor heads with no electrical conductors. In previous work,¹³ in which the cell walls were optically heated, much of the heating light was scattered and/or reflected from the cell surface, resulting in inefficient heating; several hundred milliwatts of light power was required to heat the cells to their operating temperature. This problem was exacerbated by poor thermal isolation of the cell from the supporting frame. We describe here a low-power, fiber-optically coupled optical magnetometer based on microfabricated ⁸⁷Rb vapor cells, in which the vapor cell was heated by absorption of light by filters attached to the cell windows. Attention to thermal design and vacuum packaging allowed the cells to be heated to their operating temperature with less than 150 mW of input optical power per sensor in a room-temperature environment.

One such sensor head is shown in Figure 1(a) and was assembled from several layers of micromachined silicon, each 0.5 mm to 2 mm thick. A schematic illustrating the overall design is shown in Figure 1(b). At the center of the sensor was a micromachined alkali vapor cell (not shown in Figure 1(a)) of interior volume (1.5 mm)³, containing isotopically pure ⁸⁷Rb, and a buffer gas of N₂ at a number density of about 1 amagat. The optical heating was accomplished by attaching an optical filter to each window of the cell. The two filters were made from Schott RG-9¹⁷ colored glass that absorbs light at 1.5 μm with an attenuation length of approximately 0.3 mm, while largely transmitting light at the wavelength of the Rb D1 line at 795 nm. The filter thicknesses of 0.25 mm for the entrance window and 1 mm for the exit window for the heating light were chosen such that equal amount of the incident optical power was absorbed in each filter. The absorption of the 1.5 μm light allowed the cell to be heated to an operating temperature of 150 °C, as measured by the

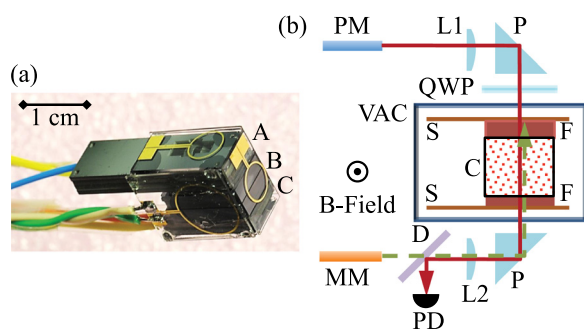


FIG. 1. (a) Photograph of the microfabricated, fiber-optically coupled magnetometer sensor head. The volume of a cuboid that would entirely enclose the assembled sensor head is 0.36 cm^3 . The probe light fiber is held in structure A, the cell in structure B, and the photodetector and heating light fiber in structure C. (b) Schematic of the sensor head assembly, showing the vapor cell illuminated from above by the probe light (solid red line) and from below by the heating light (dashed green line). PM: Polarization-maintaining optical fiber; MM: multi-mode optical fiber; L1, L2: lenses; P: reflecting prisms; QWP: quarter-wave plate; VAC: evacuated enclosure; S: polyimide web; F: optical filter; C: vapor cell; D: dichroic mirror; PD: photodiode.

on-resonance optical absorption by unpolarized atoms, with an incident power of 140 mW .

In order to thermally isolate the cell from the environment, the cell substructure was mounted using low-outgassing epoxy on a $50 \mu\text{m}$ thick polyimide web that suspended the cell from a micromachined layered silicon/glass/silicon frame.¹⁸ In order to reduce the distance between the sensing volume and the outer surface of the sensor-head to 2.5 mm , the cell was positioned off-center with respect to the frame in the plane perpendicular to the direction of propagation of the light. The sensitive volume could be placed very close to a magnetic field source which results in increased magnetic signal strength compared, for example, with SQUID magnetometers that usually require a much larger stand-off distance. The suspended cell was sealed within an evacuated enclosure formed by anodically bonding two borosilicate glass windows to the silicon frame. A small quantity of barium deposited inside the enclosure and activated under vacuum during the bonding process, served as a getter to maintain a light vacuum around the cell and reduce conduction and convection of heat from the cell to the frame. We estimate that at cell temperatures above 150°C , radiation was a major contributor to the heat loss from the cell. In addition to decreasing the operating power, good thermal isolation between the cell and the environment is important for magnetic measurements of many biological samples (such as the human body) that cannot be placed in direct contact with the heated cell without being damaged.

Probe light at 795 nm from a distributed feedback (DFB) laser was coupled into the cell from a polarization-maintaining single-mode optical fiber. Light transmitted through the cell was focused and redirected by a dichroic mirror onto a silicon PIN photodiode attached to the bottom of the structure, as illustrated in Figure 1(b). The current from the sensor photodiode was carried through a twisted pair of wires to a remotely located transimpedance amplifier. A multi-mode optical fiber with a core diameter of $200 \mu\text{m}$ coupled light at $1.5 \mu\text{m}$, originating from a diode laser and amplified by an Er-doped fiber amplifier, to the cell. This

light was transmitted to the sensor head through the dichroic mirror such that it was counter-propagating with the probe light and absorbed by the optical filters mounted on the cell. No active control of the heating light power or the probe laser power or frequency was implemented for operation of the sensor in the laboratory environment, although we anticipate such control would be needed for operation in the field, where larger temperature variation is present.

The cell temperature was sufficiently high that at ambient fields under $1 \mu\text{T}$, relaxation due to spin-exchange collisions, which is often dominant at high temperatures, was strongly suppressed.⁶ The on-resonance circularly polarized light optically pumped the atoms and created a zero-field resonance as a function of magnetic field in the transmitted power.¹⁹ The inset of Figure 2 shows the magnetic resonance as the fractional transmission of the probe light. A dispersive resonance is created through the application of an AC magnetic field transverse to the direction of propagation of the probe light oscillating at a frequency of 1.8 kHz and with an amplitude of 250 nT . This field was applied by a pair of lithographically patterned Helmholtz coils located on the outer surface of the sensor, and shown in Figure 1(a). Phase-sensitive detection at the first harmonic allows for operation at zero field with high signal-to-noise ratio.

The sensitivity of the magnetometer was measured by placing the sensor in a five-layer cylindrical magnetic shield. The shield was made of high-permeability metal except the innermost layer which was assembled from ferrite.²⁰ The shielding factor was estimated to be $>10^5$, and the thermal magnetic field noise²¹ originating from the innermost metallic shield layer was estimated to be $6 \text{ fT}/\sqrt{\text{Hz}}$. The reduction of the magnetic noise originating with the metal layers by the ferrite layer was unknown, but the sensor noise was measured to be a factor of three above this thermal noise estimate, and the in-phase and out-of-phase noise levels were similar, indicating that the shield noise was not limiting the measurement.

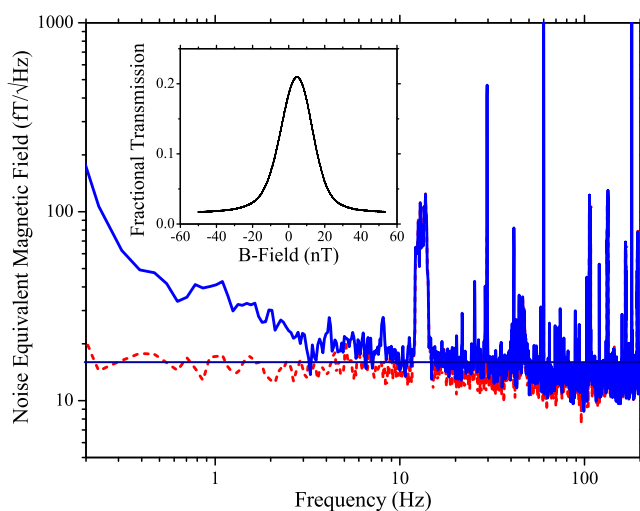


FIG. 2. Noise equivalent magnetic field measured in the sensor for the in-phase (blue solid line) and out-of-phase (red dashed line) lock-in output signals. The solid straight line shows a sensitivity of $16 \text{ fT}/\sqrt{\text{Hz}}$. The inset shows a typical magnetic resonance signal as the fractional optical power transmitted through the vapor cell as a function of magnetic field.

The DC field inside the shield was tuned to approximately zero, and the noise in the lock-in output was measured to characterize the sensitivity. The noise spectrum from both in-phase and out-of-phase lock-in signals is shown in Figure 2. Excluding a few environment-related narrow-band peaks, the sensor noise is below $20 \text{ fT}/\sqrt{\text{Hz}}$ in the band from 15 Hz to 100 Hz, increasing at low frequencies to above $1 \text{ pT}/\sqrt{\text{Hz}}$ at 0.1 Hz. The relative intensity noise of the laser was -130 dB/Hz at the detected power level of $20 \mu\text{W}$, which is about a factor of two higher than the calculated photon shot-noise for this power. The photon-shot-noise-limited sensitivity of the magnetometer is therefore about $8 \text{ fT}/\sqrt{\text{Hz}}$.

The sensitivity of $20 \text{ fT}/\sqrt{\text{Hz}}$ is considerably better than earlier fiber-optically coupled micromachined magnetometers,²² particularly at low frequencies, because the probe light is detected with a photodiode placed directly on the sensor head as opposed to being coupled off the sensor with an optical fiber. This design change results in a higher detection efficiency of the power transmitted through the cell and reduced noise due to propagation through the fiber itself. However, the sensitivity is also a factor of four worse than previous measurements using microfabricated vapor cells in table-top experiments,¹² which used independent, orthogonally propagating pump and probe fields, and optical polarimetry. This degradation in sensitivity is a result of two main factors: (a) the inability to independently optimize the detunings of the pump and probe fields, and (b) the lower signal-to-noise ratio obtained with absorption measurements compared with polarimetry. The resonance widths here are about the same as those in Ref. 12. We note that the considerably better sensitivities obtained in other experiments² are due in part to much narrower magnetic resonances in the much larger vapor cells, and in part to better signal-to-noise detection of the resonances through polarimetry.

The magnetometer could be operated at the sensitivity levels described above with 140 mW of heating light power at the output of the fiber amplifier. This is an improvement over previous sensor designs,¹³ in which the volume surrounding the sensor head was not evacuated and required about 450 mW of heating power for steady-state operation at 150°C . From measurements of the cell heating with a free-space laser before assembly of the integrated optics, we estimate that 15% of this heat laser power is not coupled as heat into the cell assembly, but is instead lost due the optical fiber interconnects, reflections from glass surfaces, and misalignment of heating light on the sensor. We estimate that the power conducted through the tethers at the operating temperature is below 5 mW. We consider black-body radiation to be an important limit for power dissipation in these types of sensors, which the device described here has come close to reaching. According to the Stefan-Boltzmann law, a rectangular cuboid at 150°C of dimensions $2.5 \text{ mm} \times 2.5 \text{ mm} \times 3.35 \text{ mm}$ with an emissivity of unity radiates 65 mW into an ambient temperature of 20°C . While low-emissivity coatings and baffles can be used to reduce the radiated power further, such design features may be expensive to implement in a microfabricated device technology that is broadly used in real-world applications. The remainder of the dissipated power (about 50 mW) is presumably lost through the conduction of heat through residual gas in the evacuated enclosure,

although further studies are needed to confirm this hypothesis. We believe that this last heat loss mechanism can be entirely mitigated with an improved vacuum packaging process.

Three additional sensors similar to that shown in Figure 1(a) were fabricated and operated together with the first. All four sensors were simultaneously driven by a single heating laser and a single probe laser, with the light from each laser divided between the sensors with 1×4 fiber-optic splitters. The optical power levels transmitted to each sensor for each wavelength were adjusted once at the beginning of the measurement with a mechanical control on the splitter and not adjusted subsequently. The sensors were modulated at frequencies mutually differing by more than 200 Hz to avoid cross-talk. All sensors achieved a sensitivity below $25 \text{ fT}/\sqrt{\text{Hz}}$ in the band 15 Hz–100 Hz and below $100 \text{ fT}/\sqrt{\text{Hz}}$ at 1 Hz.

We anticipate this sensor technology will be important for a variety of biomagnetic measurements, including measurements of heart and brain magnetic fields. The approximate magnitude of these fields measured outside the body is in the range of 100 pT and 1 pT, respectively, and the required measurement bandwidths are on the order of 500 Hz. The sensor technology demonstrated here will be much less expensive to produce and less cumbersome to operate than the SQUID-based magnetometer technology used almost exclusively for these measurements until now. Figure 3 shows a comparison of the magnetometer sensitivity obtained here with the typical sensitivity of magnetometers in a commercial SQUID-based magnetoencephalography system²³. Also shown is the typical brain field signal, including the “alpha rhythm” peak at 10 Hz, estimated from SQUID measurements and renormalized for the closer stand-off distance made possible by the small size of the sensor.²⁴ We therefore anticipate that the sensor described here could detect real-time (i.e., with no averaging) brain alpha-rhythm

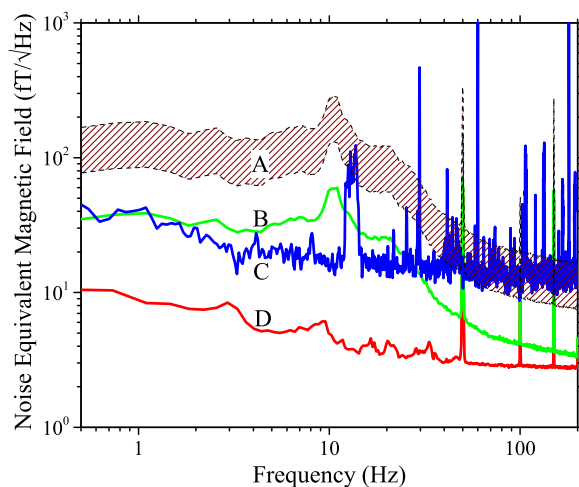


FIG. 3. Comparison of the equivalent magnetic noise measured with our optical magnetometers (Trace C, blue) with that of a typical commercial SQUID magnetometer (Trace D, red). Also shown is the average of the spectra of 102 SQUID magnetometers in a helmet-shaped sensory array positioned 18 mm above the scalp, measuring the magnetic field produced by a typical human brain (Trace B, green). The red hatched region (A) shows the expected enhancement of this brain spectrum for a sensor placed 2.5 mm above the scalp (see Ref. 24 for additional details). The SQUID (Trace D, red) and brain field (Trace B, green) data were originally presented in Ref. 23.

activity with a signal-to-noise ratio of about 10. Medically relevant signals such as those due to epileptic activity are much larger than the “typical” brain field spectrum shown in Figure 3 and could be detected correspondingly more easily. We note that previous measurements²⁵ using similar sensors with a sensitivity ~ 200 fT/ $\sqrt{\text{Hz}}$ clearly resolved alpha-rhythm activity with no averaging; a broader range of MEG signals and features could be resolved with the sensor described here because of its improved sensitivity.

In conclusion, we have developed a low-power, micro-fabricated, fiber-optically coupled sensor head that achieves a sensitivity below 20 fT/ $\sqrt{\text{Hz}}$. Four such sensors were fabricated, each running on less than 150 mW of heating power, and operated simultaneously with a single pair of heating and probe lasers. This type of instrument offers increased potential for low-cost production because of the lithographically defined silicon structure and may be particularly important in applications where large numbers of sensors are needed, such as biomagnetic imaging.

Funding from DARPA Defense Sciences Office and NIST is acknowledged. The authors also gratefully acknowledge valuable fabrication support from Susan Schima and thank Professor L. Parkkonen for helpful comments and for the data presented in Figure 3. This work is a contribution of NIST, an agency of the U.S. Government, and is not subject to copyright.

- ¹H. G. Dehmelt, *Phys. Rev.* **105**, 1487 (1957); D. Budker and M. Romalis, *Nat. Phys.* **3**, 227 (2007).
²H. B. Dang, A. C. Maloof, and M. V. Romalis, *Appl. Phys. Lett.* **97**, 151110 (2010).
³D. Sheng, S. Li, N. Dural, and M. V. Romalis, e-print arXiv:1208.1099v1.
⁴A. Nagel, L. Graf, A. Naumov, E. Mariotti, V. Biancalana, D. Meschede, and R. Wynands, *Europhys. Lett.* **44**, 31 (1998); Z. M. Li, R. T. Wakai, and T. G. Walker, *Appl. Phys. Lett.* **89**, 134105 (2006).
⁵M. V. Balabas, T. Karaulanov, M. P. Ledbetter, and D. Budker, *Phys. Rev. Lett.* **105**, 070801 (2010).
⁶J. C. Allred, R. N. Lyman, T. W. Kornack, and M. V. Romalis, *Phys. Rev. Lett.* **89**, 130801 (2002).

- ⁷M. Vengalattore, J. M. Higbie, S. R. Leslie, J. Guzman, L. E. Sadler, and D. M. Stamper-Kurn, *Phys. Rev. Lett.* **98**, 200801 (2007).
⁸V. M. Acosta, E. Bauch, A. Jarmola, L. J. Zipp, M. P. Ledbetter, and D. Budker, *Appl. Phys. Lett.* **97**, 174104 (2010).
⁹J. M. Higbie, E. Corsini, and D. Budker, *Rev. Sci. Instrum.* **77**, 113106 (2006).
¹⁰P. D. D. Schwindt, S. Knappe, V. Shah, L. Hollberg, J. Kitching, L. A. Liew, and J. Moreland, *Appl. Phys. Lett.* **85**, 6409 (2004).
¹¹P. D. D. Schwindt, B. Lindseth, S. Knappe, V. Shah, J. Kitching, and L.-A. Liew, *Appl. Phys. Lett.* **90**, 081102 (2007).
¹²W. C. Griffith, S. Knappe, and J. Kitching, *Opt. Express* **18**, 27167 (2010).
¹³J. Preusser, V. Gerginov, S. Knappe, and J. Kitching, in *IEEE Sensors Conference* (IEEE, 2008), p. 344.
¹⁴S. Knappe, T. H. Sander, O. Kosch, F. Wiekhorst, J. Kitching, and L. Trahms, *Appl. Phys. Lett.* **97**, 133703 (2010).
¹⁵G. Bison, R. Wynands, and A. Weis, *Opt. Express* **11**, 904 (2003); M. N. Livanov, A. N. Kozlov, S. E. Sinelnikova, J. A. Kholodov, V. P. Markin, A. M. Gorbach, and A. V. Korinewsky, *Adv. Cardiol.* **28**, 78 (1981).
¹⁶H. Xia, A. B. A. Baranga, D. Hoffman, and M. V. Romalis, *Appl. Phys. Lett.* **89**, 211104 (2006).
¹⁷Trade name is stated for technical clarity and does not imply endorsement by NIST. Products from other manufacturers may perform as well or better.
¹⁸M. J. Mescher, R. Lutwak, and M. Varghese, in *Solid-State Sensor, Actuator and Microsystems Workshop* (Seoul, Korea, 2005), p. 311.
¹⁹J. Dupont-Roc, S. Haroche, and C. Cohen-Tannoudji, *Phys. Lett. A* **28**, 638 (1969).
²⁰T. W. Kornack, S. J. Smullin, S. K. Lee, and M. V. Romalis, *Appl. Phys. Lett.* **90**, 223501 (2007).
²¹T. Varpula and T. Poutanen, *J. Appl. Phys.* **55**, 4015 (1984).
²²R. R. Mhaskar, S. Knappe, and J. Kitching, in *Proceedings of the IEEE International Frequency Control Symposium* (IEEE, Newport Beach, CA, 2010), pp. 376.
²³L. Parkkonen, Ph.D. dissertation, Helsinki University of Technology, 2009.
²⁴The brain field noise spectrum shown in Figure 3 B is an average of the magnetic field measured with 102 SQUID magnetometers in a helmet-shaped sensor array placed 18 mm from the scalp. Environmental interference in this data as suppressed with signal-space projection (SSP) prior to computing the spectra. We assume the signal originated from a current dipole field source situated in the range 2 cm to 5 cm below the scalp and calculate the expected increase in the measured signal for a sensor placed 2.5 mm above the scalp. This leads to an improvement by a factor of 2.2 to 4.8 in the signal strength at the closer location. The resulting enhanced brain signal is shown by the red hatched region A in Figure 3.
²⁵T. H. Sander, J. Preusser, R. Mhaskar, J. Kitching, L. Trahms, and S. Knappe, *Biomed. Opt. Express* **3**, 981 (2012).